

Contribution of viscous stress work to wall heat flux in compressible turbulent channel flowsPeng Zhang  and Zhenhua Xia ^{*}*Department of Engineering Mechanics, Zhejiang University, Hangzhou 310027, China*

(Received 30 June 2020; accepted 6 October 2020; published 26 October 2020)

In this paper we derive an exact expression for the mean heat flux at the wall for the compressible turbulent channel flow. In the expression, the heat flux at the wall can be decomposed into four parts, including the contribution from the turbulent heat transfer, the contribution from the molecular heat transfer, the contribution from the pressure work, and the contribution from the work from viscous stress (VW). The decomposition is validated in compressible turbulent channel flows with isothermal walls at three different Reynolds and Mach numbers, and the results match very well with the direct estimations at the wall. The data also show that the VW term dominates the contributions (around 90%) in the decomposition while around 90% of VW is from the near-wall region ($y/h < 0.2$), illustrating the importance of the viscous stress work in the near-wall region.

DOI: [10.1103/PhysRevE.102.043107](https://doi.org/10.1103/PhysRevE.102.043107)**I. INTRODUCTION**

Compressible wall-bounded turbulence is of great importance in many industrial and engineering applications [1,2]. In the past decades, plenty of effort has been devoted to study the effect of compressibility and the corresponding mechanism on wall-bounded turbulence [3–6]. In compressible wall-bounded turbulence, the heat transfer is also a very important topic besides the flow velocity field, making the wall resistance and the heat flux at the wall to be two critical quantities.

In the past, researchers have documented that the skin friction in wall-bounded turbulence can be expressed as the contribution from the flow statistics inside the flow domain [7–10]. Fukagata *et al.* [7] first derived a simple expression of the componential contribution from different dynamical effects to the surface friction resistance based on a streamwise momentum budget in the wall reference frame in incompressible channel, pipe, and plane boundary layer flows. The expression shows that four parts, including the laminar, turbulent, inhomogeneous, and transient components, will contribute to the local skin friction (FIK decomposition). Furthermore, the turbulent term is a weighted integral of the Reynolds stress distribution, and the near-wall Reynolds stress contributes dominantly. Based on the above fact, Fukagata *et al.* [7] used the above decomposition to analyze the drag modification by the opposition control and by the uniform wall blowing and suction. Gomez *et al.* [8] extended the FIK decomposition to compressible wall-bounded flows, and it was reported that two additional compressibility-induced terms, namely, the compressible contribution term and the compressible turbulent interaction term, will come out besides the laminar and turbulent terms in incompressible channel flows. Their numerical data in compressible turbulent channel flows at different Mach numbers showed that the main con-

tribution to the skin friction is still from the turbulent term, while the two additional compressibility-induced terms are quasinegligible. Recently, the FIK decomposition and its compressible extension were used to form a new quadrant analysis for wall-bounded turbulence [11] and to study the genuine compressibility effect in compressible channel flows [12]. Renard and Deck [9] derived another decomposition (RD decomposition) of the mean skin friction from a mean streamwise kinetic-energy budget in an absolute reference frame for incompressible wall-bounded turbulence. In an incompressible zero-pressure-gradient smooth-flat-plate boundary layer flow, the local skin friction, which can also represent the mean power supplied by the wall to the fluid in the absolute frame, can therefore be decomposed into a diffusion term, which diffuses through the boundary layer profile with a direct viscous dissipation, a dissipation term, which is dissipated by all the production of the turbulent kinetic energy, and an inhomogeneous term, which represents the spatial growth of the flow or the rate of the gain of mean streamwise kinetic energy by the fluid in the absolute frame. For incompressible turbulent channel flows, the RD decomposition can also be derived from the argument of dissipation function [13–15]. Recently, the RD decomposition was extended to compressible turbulent channel flows [16] and compressible zero-pressure-gradient boundary flows [17] to investigate the effect of Reynolds number and scalings of each term.

For heat flux at the wall, a great deal of work has been done, too. Morinishi *et al.* [18], Shadloo *et al.* [19], and Liang and Li [20] studied the statistics of wall heat transfer at different temperature boundaries, including adiabatic and isothermal walls, while Kawamura *et al.* [21] and Duan *et al.* [22] investigated the Reynolds and Prandtl number effects on the turbulent heat transport and wall heat flux in different wall temperatures. The scaling of the velocity profile under wall heat transfer for compressible turbulent boundary layers was also studied by Zhang *et al.* [23]. Other researchers tried to quantify it from the skin friction. Hopkins and Inouye [24] introduced a formula to predict the heat transfer at the wall from the

^{*}xiazh@zju.edu.cn

skin friction on flat plate at supersonic and hypersonic Mach numbers. For fully developed compressible turbulent channel flows with equal isothermal boundary conditions, Huang *et al.* [25] found

$$q_w \equiv -\lambda \left. \frac{d(T)}{dy} \right|_w = -u_b \tau_w, \quad (1)$$

based on the argument that the overall energy balance in a fully developed channel flow requires that the total pressure work done (or the total heat generation) across the channel equal and the heat transfer into the walls is the same. Here λ is the thermal conductivity, $u_b = \int_0^h \langle \rho u \rangle dy / \int_0^h \langle \rho \rangle dy$ is the bulk velocity, and τ_w is the wall shear stress. This formula was also discovered by Ghosh *et al.* [26] and Li *et al.* [16]. For adiabatic thermal boundary conditions, the above formula (1) is invalid locally. Furthermore, the above works are all devoted to estimate the quantity of the heat transfer at the wall. Not many of them tried to unravel the source of the heat transfer at the wall, although the balance equation was derived in Ghosh *et al.* [26] to explain the difference in the mean density and temperature profiles in channel and pipe flows.

In fact, Fukagata *et al.* [27] used to derive a mathematical relation of the contribution of turbulent heat flux to the Nusselt number for incompressible wall-bounded turbulence with isothermal and isoflux conditions. Based on the derived relation, they proposed a strategy for simultaneous control to achieve friction drag reduction and heat transfer augmentation in a fully developed incompressible turbulent channel flow [28]. Nevertheless, the work was based on the transport equation of the temperature, which is a passive scalar for the incompressible velocity field. For compressible cases, the temperature is no longer a passive scalar but coupled with the velocity field, the source of the heat transfer at the wall is still unknown. In the present paper we derive a direct mathematical relation between the heat flux at the wall and the integral of the turbulent statistics inside the flow field for compressible turbulent channel flows. Similar to the decomposition of skin friction, the decomposition of the heat flux at the wall could show its direct sources and the possible dominant contributions, which might be useful for flow control.

II. EXACT MATHEMATICAL DECOMPOSITION OF THE WALL HEAT FLUX q_w

In this section we are going to derive the decomposition of the wall heat flux q_w in a fully developed compressible turbulent channel flow, as sketched in Fig. 1. The compressible fluid is driven by a uniform force along the streamwise direction, and it flows between two infinite parallel walls. The magnitude of the force is adjusting in time to ensure a constant flow flux in the streamwise direction. In the simulations, a computational box of size $L_x \times L_y \times L_z$ is adopted, and periodic boundary conditions are applied in the wall-parallel directions (streamwise and spanwise directions), while the no-slip boundary conditions are adopted for the velocity fields at both walls. It is worth noting that the no-slip boundary condition restriction is not needed for the wall-normal velocity component in the following derivation of the formulas for the wall heat flux q_w

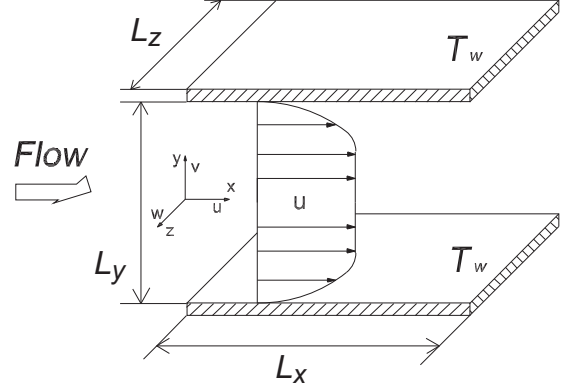


FIG. 1. Schematic diagram of turbulent flow in compressible channel without blowing nor suction at the wall. Please note that we may allow blowing and/or suction at the wall, as what was done by Kametani *et al.* [29].

and it will be removed to allow the blowing and/or suction at the wall, as was done by Kametani *et al.* [29]. In the present paper only isothermal boundary conditions at both walls are considered for the temperature field, and it is T_w equally. Under these assumptions, it can be inferred that the field is symmetric with respect to the center plane. In the derivation only the internal energy equation will be used, and it reads as follows [30]:

$$\frac{\partial e}{\partial t} + \frac{\partial(eu_k)}{\partial x_k} + \frac{\partial q_k}{\partial x_k} = -p \frac{\partial u_k}{\partial x_k} + \tau_{ij} \frac{\partial u_i}{\partial x_j}, \quad (2)$$

where

$$\tau_{ij} = \mu \left(\frac{\partial u_i}{\partial x_j} + \frac{\partial u_j}{\partial x_i} - \frac{2}{3} \frac{\partial u_k}{\partial x_k} \delta_{ij} \right), \quad q_k = -\lambda \frac{\partial T}{\partial x_k}. \quad (3)$$

Here, $e = p/(\gamma - 1) = \rho C_v T$ is the internal energy for the unit volume, with C_v being the specific heat at constant volume, u_1, u_2 , and u_3 denote the streamwise (x_1 or x), wall-normal (x_2 or y), and spanwise (x_3 or z) velocity fluctuations, respectively; u, v, w are used interchangeably with u_1, u_2, u_3 . It should be emphasized that the forcing term has disappeared in the internal energy equation, since the forcing term directly changes only the kinetic energy. Nevertheless, it will modify the internal energy indirectly through the pressure dilatation term,

$$P_d = -p \frac{\partial u_k}{\partial x_k},$$

and the viscous action term,

$$V_a = \tau_{ij} \frac{\partial u_i}{\partial x_j},$$

which are the interaction terms between the kinetic and internal energy [30]. If we considered the total energy equation, the forcing term would appear [31]. Equation (2) can be averaged using the Reynolds averaging operator ($\bar{\cdot}$) to obtain the Reynolds-averaged equation for the internal energy

$$\frac{\partial \bar{e}}{\partial t} + \frac{\partial(\bar{e}u_k)}{\partial x_k} + \frac{\partial \bar{q}_k}{\partial x_k} = \bar{P}_d + \bar{V}_a. \quad (4)$$

For a fully developed turbulent channel flow, the Reynolds averaging operator can be substituted by the averaging in x , z , and t , and thus

$$\frac{\partial \bar{\phi}}{\partial x} = \frac{\partial \bar{\phi}}{\partial z} = \frac{\partial \bar{\phi}}{\partial t} = 0$$

for any quantity ϕ . The corresponding fluctuation is denoted as $\phi' = \phi - \bar{\phi}$. Equation (4) could be further simplified as

$$\frac{\partial(\bar{e}v)}{\partial y} + \frac{\partial \bar{q}_y}{\partial y} = \bar{P}_d + \bar{V}_a. \quad (5)$$

By integrating Eq. (5) from 0 to y , we obtain

$$\bar{q}_y + \bar{e}v - (q_w + \bar{e}v|_{y=0}) = \int_0^y \bar{P}_d dy + \int_0^y \bar{V}_a dy. \quad (6)$$

Equivalently,

$$q_w = \bar{q}_y + \bar{e}v - \int_0^y \bar{P}_d dy - \int_0^y \bar{V}_a dy - \bar{e}v|_{y=0}. \quad (7)$$

Equation (7) shows that the wall heat flux can be evaluated from the information within the region $[0, y]$ inside the field and the blowing and/or suction information at the wall. It should be noted that the above equation was also obtained by Ghosh *et al.* [26] to explain the difference of mean temperature and density in the wall-normal direction. By integrating Eq. (7) from 0 to h (h being the half-width of the channel), we obtain the following relationship:

$$\begin{aligned} q_w = & \underbrace{\frac{1}{h} \int_0^h \bar{q}_y dy}_{\text{MH}} + \underbrace{\frac{1}{h} \int_0^h C_v \bar{\rho} T'' v'' dy}_{\text{TH}} + \underbrace{\frac{1}{h} \int_0^h (y-h) \bar{P}_d dy}_{\text{PW}} \\ & + \underbrace{\frac{1}{h} \int_0^h (y-h) \bar{V}_a dy}_{\text{VW}} \\ & + \underbrace{\frac{1}{h} \int_0^h C_v \bar{\rho} \{T\} \{v\} dy - C_v \bar{\rho} T v \Big|_{y=0}}_{\text{BS}}. \end{aligned} \quad (8)$$

Here the Favre averaging operator $\{\phi\} = \bar{\rho\phi}/\bar{\rho}$ is adopted and $\phi'' = \phi - \{\phi\}$ is the corresponding fluctuations. This relation shows that the heat flux at the wall can be decomposed into five contributing terms: the contribution from the turbulent heat transfer (TH), the contribution from the molecular heat transfer (MH), the contribution from the pressure work (PW), the contribution from the work from viscous stress (VW), and the contribution due to the blowing and/or suction at the walls (BS). If there is no blowing and suction at the walls, $\{v\} = 0$ in the whole channel and the BS term will disappear. It is seen that the MH and TH terms are the volume average of the molecular heat transfer and the turbulent heat transfer in the wall-normal direction, respectively, while the PW and VW terms are the weighted average of the pressure dilatation and the viscous action terms, respectively, where the weight is linearly decreasing with the distance from the wall. It is worth noting that Eqs. (7) and (8) deliver different information on q_w . Equation (7) can be viewed as a local balance equation, and it can be used to evaluate q_w at any local y . In applications, the dominating contribution term to q_w may be different at

different y (see Fig. 9 in Ghosh *et al.* [26]). Equation (8) is the wall-normal average of Eq. (7), and it can provide the information on the amount of the contribution from each term to q_w in an average sense. More importantly, the contributions from the pressure dilatation and the viscous action are the integrals of \bar{P}_d and \bar{V}_a in the interval $[0, y]$ in Eq. (7). Although they can give the amount of the contributions at any y , the results might hide the underlying physics. For example, according to results in Ghosh *et al.* [26], the relative contribution from the viscous action (the summation of the direct dissipation and the turbulent dissipation) based on Eq. (7) increases with y . However, the term \bar{V}_a in fact decreases with y [see the hint from Fig. 5(b) below], and thus the contribution from the viscous work should be more important in the near-wall region. This physical information about the contribution of the viscous action can be correctly expressed through Eq. (8) (see Figs. 5 and 7 below and the related discussions). Actually, when Eq. (7) is integrated, the integral interval can be arbitrary and a different interval can deliver a different message. Nevertheless, the half-channel integral is unique and it uses the information from the whole channel. The difference between Eqs. (7) and (8) is very similar to what was done for the skin friction in incompressible [7] and compressible [8] wall-bounded turbulence, where the authors integrated the momentum balance equations to obtain the decomposition formulas for the skin friction. It should also be noted that the decomposition can be derived for compressible turbulent pipe flows and turbulent boundary layers following the same procedure.

III. NUMERICAL SIMULATION

Direct numerical simulations (DNS) are performed for three fully developed compressible turbulent channel flows. The OPENCFD code using the high-order finite difference method from Prof. Xinliang Li is used, and the code has been validated before [20,32,33]. The inviscid and viscous terms are discretized by using a seventh-order upwind scheme and an eighth-order central scheme, respectively, and the time is advanced using an explicit third-order Runge-Kutta scheme. In the simulations, the viscous coefficient μ is calculated by using Sutherland's formula, and all quantities are nondimensionalized by the reference temperature $T_{\text{ref}} = 288.15$ K, the viscosity at the reference temperature μ_{ref} , the sound speed at the reference temperature c_0 , h , the bulk-averaged density $\rho_m = \int_0^2 \bar{\rho} dy / 2$, and the bulk velocity $u_m = \int_0^2 \bar{\rho} u dy / (2\rho_m)$. The control parameters are the Reynolds number Re and the Mach number Ma , and they are defined as

$$\text{Re} = \frac{\rho_m u_m h}{\mu_{\text{ref}}}, \quad \text{Ma} = \frac{u_m}{c_0}.$$

The thermal conductivity is estimated from μ through the Prandtl number $\text{Pr} = C_p \mu / \lambda = 0.72$, with C_p being the specific heat at constant pressure.

The grid is uniform in the streamwise and spanwise directions, while it is clustered in the near-wall region in order to capture the near-wall dynamics of the streaks. Details of the flow conditions, the computational domains, the grid resolutions, as well as the wall heat flux coefficient are listed in Table I. It is seen that our grid resolutions in the wall

TABLE I. Details of the flow conditions, the computational domains, and the grid resolutions. In the computation, $L_y = 2$, $\gamma = 1.4$, and $T_w = 1$. The friction Reynolds number $Re_\tau = \rho_w u_\tau h / \mu_w$ is defined using the density at the wall ρ_w , the viscosity at the wall μ_w , and the friction velocity $u_\tau = \sqrt{\tau_w / \rho_w}$, where τ_w are the wall shear stress values. Re_τ^* is the transformed friction Reynolds number using the TL transformation. $B_q = q_w / (\rho_w C_p u_\tau T_w)$ is the wall heat flux coefficient, and $1 / (\rho_w C_p u_\tau T_w) = 1.691, 13.243, \text{ and } 38.475$, respectively.

Case	Re	Re_τ	Re_τ^*	Ma	B_q	L_x	L_z	N_x	N_y	N_z	Δx^+	Δz^+	Δy_{\min}^+	Δy_{\max}^+
Case 1	6000	355	332	0.5	0.0057	4π	$4\pi/3$	400	180	320	11.15	4.64	0.59	8.23
Case 2	6000	408	267	1.5	0.0451	4π	$4\pi/3$	400	180	320	12.82	5.34	0.68	10.68
Case 3	4880	456	143	3.0	0.1392	4π	$4\pi/3$	400	210	320	14.32	5.96	0.65	9.05
Coleman <i>et al.</i> [34]	4880	451	–	3.0	0.137	4π	$4\pi/3$	144	119	80	≈ 39	≈ 24	≈ 0.2	–
Modesti and Pirozzoli [35]	≈ 7500	500	–	1.5	0.042	6π	2π	1024	256	512	9.2	6.1	–	–

parallel directions are within the suggested range, and they are comparable with those used by Modesti and Pirozzoli [35] and Li *et al.* [16].

Figure 2(a) shows the mean velocity profiles from the three cases normalized using u_τ , μ_w , and ρ_w (conventional

normalization) as

$$y^+ = \frac{\rho_w u_\tau y}{\mu_w}, \quad u^+ = \frac{\langle u \rangle}{u_\tau}.$$

For comparison, the reference data from Coleman *et al.* [34] and Modesti and Pirozzoli [35] at similar Reynolds numbers and Mach numbers are also shown. It is clearly seen that our simulation results match very well with those reference data, illustrating the correctness of the present simulations. It is also evident that the mean velocity profiles at different Ma and Re apparently diverge when they are normalized following the convective normalization. Although the mean velocity profiles still exhibit a logarithmic behavior, the intercepts will increase apparently with Ma, illustrating the effect of compressibility. According to Trettel and Larsson [36], if the new transformation (TL transformation),

$$Y^+ = \frac{\bar{\rho}(\tau_w / \bar{\rho})^{1/2} y}{\bar{\mu}}, \quad (9)$$

$$U^+ = \int_0^{u^+} \left(\frac{\bar{\rho}}{\rho_w} \right)^{1/2} \left[1 + \frac{1}{2} \frac{d\bar{\rho}}{\bar{\rho}} \frac{dy}{y} - \frac{1}{\bar{\mu}} \frac{d\bar{\mu}}{\bar{\mu}} \frac{dy}{y} \right] du^+, \quad (10)$$

is applied to the compressible channel flow, an excellent collapse of the mean velocity profile can be obtained at different Re, Ma, and B_q , and we plot the mean velocity profiles from the three cases using the TL transformation in Fig. 2(b). The incompressible DNS data at $Re_\tau = 395$ and $Re_\tau = 180$ from Moser *et al.* [37] are also shown for reference. It is clearly seen from the figure that the mean velocity profiles collapse very well with the reference incompressible data when the TL transformation is used, which again proves the accuracy of the present data. For case 1, the transformed friction Reynolds number $Re_\tau^* \approx 332$ and the transformed mean velocity profile match very well with the incompressible DNS data at $Re_\tau = 395$. For case 2, the TL transformed mean velocity profile shifts upwards for a little bit, and it almost coincides with the profile from the incompressible DNS at $Re_\tau = 180$. For case 3, the TL transformed profile further shifts upwards with a larger intercept in the log law region. We attribute this upshift behavior to the lower transformed friction Reynolds numbers effect, where Re_τ^* values are around 267 and 143, respectively, for cases 2 and 3. In fact, for the incompressible DNS data at lower Reynolds numbers, it was shown by Moser *et al.* [37] that the apparent log law in the $Re_\tau = 180$ case has a larger intercept than in the $Re_\tau = 395$ case [see Fig. 1 in Ref. [37] and Fig. 2(b)]. With a much lower transformed

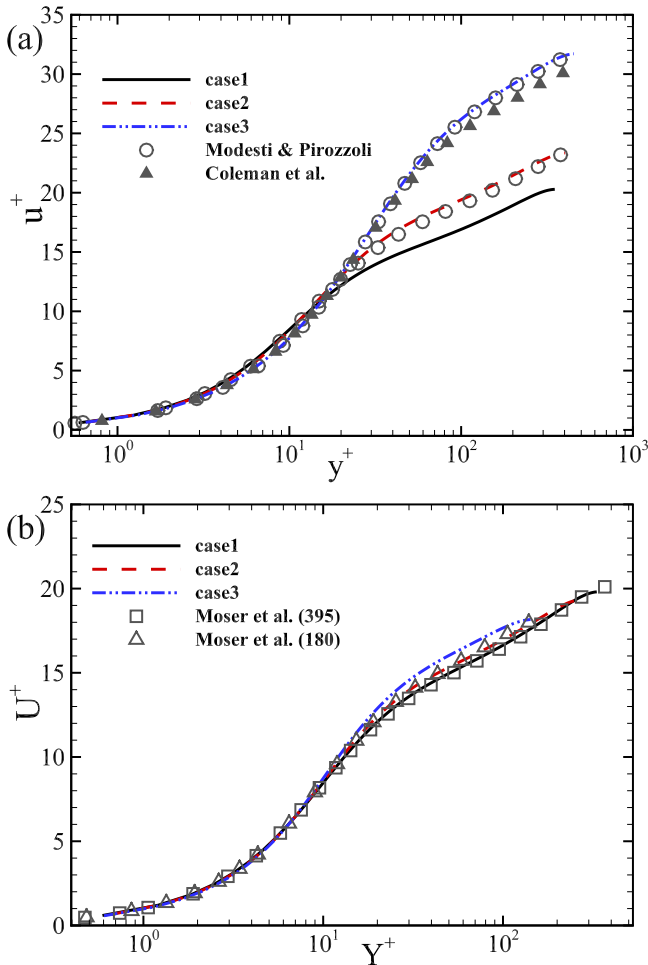


FIG. 2. (a) Mean velocity profiles from the three cases normalized using u_τ , μ_w , and ρ_w . The results from Coleman *et al.* [34] and Modesti and Pirozzoli [35] are also shown for comparison. No van Driest transformation is applied. (b) Mean velocity profiles from the three cases normalized using the Trettel and Larsson transformation [36]. The incompressible DNS results at $Re_\tau = 395$ and $Re_\tau = 180$ from Moser *et al.* [37] are also shown as reference.

TABLE II. Contribution to the wall heat flux coefficient B_q for the three different cases. The relative error is calculated by $error = |(B_{q,integral} - B_{q,direct})/B_{q,direct}|$, where $B_{q,direct}$ is calculated directly through the wall heat flux using the temperature gradient at the wall, and $B_{q,integral}$ is the summation of the four integral contributions.

Case	$B_{q,direct}$	$B_{q,integral}$	Error	TH	MH	PW	VW
Case 1	-5.702×10^{-3}	-5.758×10^{-3}	0.98%	-3.057×10^{-4}	-1.793×10^{-4}	-1.060×10^{-4}	-5.167×10^{-3}
	–	–	–	5.3095%	3.1144%	1.8414%	89.7347%
Case 2	-4.512×10^{-2}	-4.470×10^{-2}	0.93%	-2.219×10^{-3}	-1.516×10^{-3}	-7.305×10^{-4}	-4.023×10^{-2}
	–	–	–	4.9640%	3.3926%	1.6344%	90.0090%
Case 3	-1.392×10^{-1}	-1.405×10^{-1}	0.93%	-6.618×10^{-3}	-7.502×10^{-3}	-2.051×10^{-3}	-1.247×10^{-1}
	–	–	–	4.3915%	5.3415%	1.4602%	88.8068%

friction Reynolds number, it is reasonable that the mean profile further shifts upwards for case 3.

IV. RESULTS AND DISCUSSION

Now we would like to validate the proposed decomposition (8) by using our DNS data at three different Re and Ma. In the present study, no blowing and suction is applied at the wall, and thus the last BS term in Eq. (8) is zero. The other four contributions to the wall heat flux coefficient (normalized wall heat flux) and their summation as well as the direct estimation of the wall heat flux coefficient at the three cases are listed in Table II, and the relative contributions of different terms are shown in Fig. 3. It is clearly seen from the data that the decomposition in Eq. (8) is quite accurate, and the relative error is within 1% in all three cases. More importantly, the data show that the main contribution to B_q is from the VW term, and it is about 90% at three different Ma and Re cases. This is in sharp contrast to the passive scalar case for incompressible flows, where the temperature is assumed as a passive scalar and the work from the viscous stress is ignored [27]. For the other three terms, it is seen that the pressure work contributes the least, which is around 1.5%, while the TH and MH terms contribute around 4%–5% and

3%–5% for the three cases considered. When Ma increases, the contributions from all four terms increase. Nevertheless, the relative contributions show different behaviors, where the relative contribution from the TH and PW terms decrease while the relative contribution from the MH term increases. If we assumed the thermal conductivity was constant, then the MH term could be related to the temperature differences ΔT between the channel center and the wall. Although the thermal conductivity varies in space and time, we still can infer that it can be related to ΔT . At the present three cases, ΔT increases with Ma, which is in the same trend as the contribution of the MH term.

To further understand the VW term, $\overline{V_a}$ can be decomposed to a mean part and a fluctuating part, which is the viscous dissipation, as in the following equation [25]:

$$\overline{V_a} = \overline{\tau_{i2}} \frac{\partial \overline{u_i}}{\partial y} + \overline{\tau'_{ij}} \frac{\partial u'_i}{\partial x_j}. \quad (11)$$

Accordingly, the VW term can be decomposed into a mean part VWm and a fluctuating part VWf. The magnitudes of the two terms at the three cases are also shown in Fig. 3. In the present cases, it is seen that the contributions from the VWm term are larger than the VMf term, where the former contribute more than 50% of the total wall heat flux. Furthermore, the VWm term increases with Ma while the VWf term shows an opposite trend.

We now turn to the wall-normal distributions of the four integrands in Eq. (8). Figure 4 shows the normalized wall-normal distributions of the integrands in the TH and MH terms. As already discussed above, the TH term is the wall-normal average of the turbulent heat transfer $C_v \rho T'' v''$, while the MH terms is the wall-normal average of the molecular heat transfer $\overline{q_y}$. As shown in Fig. 4, when normalized with the same nondimensionalized parameter $\rho_w C_p u_\tau T_w$ as B_q , the wall-normal distributions of $C_v \rho T'' v''$ and $\overline{q_y}$ diverge for the three cases, although they have the same shapes. For the normalized $C_v \rho T'' v''$, it is zero at $y = 0$ and 1 and negative in between. When Ma increases, the absolute value of the peak increases while the location of its peak also moves away from the wall. This is consistent with the increase of the TH term (absolute value), as listed in Table II. For the normalized $\overline{q_y}$, it is B_q at the wall and then it (the absolute value of $\overline{q_y}$) decreases to zero rapidly as y increases, which makes the contribution from the MH term (the wall-normal average of $\overline{q_y}$) rather small, and the wall heat flux has to be compensated by the

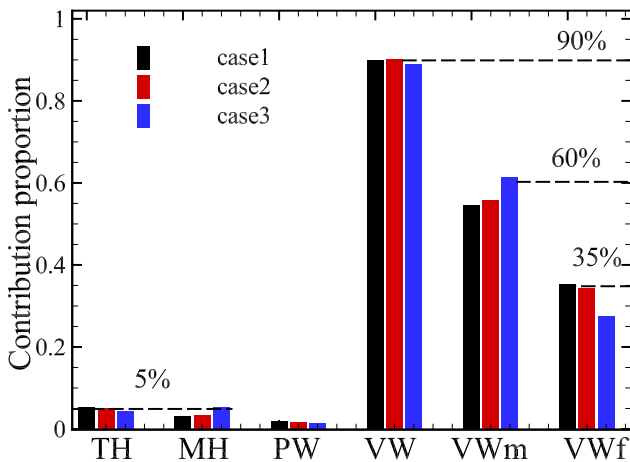


FIG. 3. Relative contribution of the four different terms to the wall heat flux coefficient. The mean part and fluctuation part from the VW term are also shown.

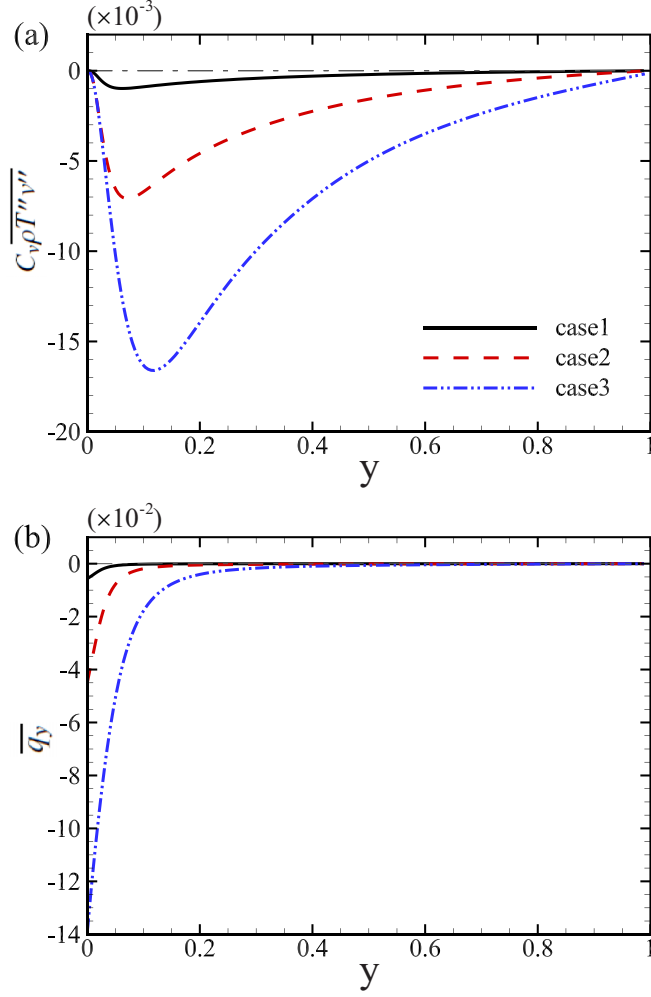


FIG. 4. Wall-normal distributions of (a) $C_v \overline{\rho T'' v''}$ and (b) $\overline{q_y}$ from the three cases. The quantities are normalized with $\rho_w C_p u_\tau T_w$.

other three terms. Clearly, the normalized $\overline{q_y}$ increases with Ma.

Figure 5 shows the weighted wall-normal distributions of the integrands in the PW and VW terms. The wall-normal distributions of $\overline{P_d}$ and $\overline{V_a}$ are quite similar to $(1-y)\overline{P_d}$ and $(1-y)\overline{V_a}$, which is due to the fact that $\overline{P_d}$ and $\overline{V_a}$ are very close to zero in the core region ($0.4 < y/h < 1$) and the weight $1-y$ is a linear with y , and they will not be shown here. For the normalized $(1-y)\overline{P_d}$, there is a positive peak at around $y/h \approx 0.05$ and a negative peak further away from the wall. The absolute values of the two peaks and their locations increase with Ma. For the normalized $(1-y)\overline{V_a}$, it is very large at the wall and then decreases rapidly to zero as y increases for all three cases. The values are much larger at higher Ma.

Figures 6 and 7 show the cumulative contributions of the integrands in the TH, MH, PW, and VW terms from the three cases. They are defined as

$$\text{Th}(y) = \int_0^y C_v \overline{\rho T'' v''} dy^* / \int_0^1 C_v \overline{\rho T'' v''} dy^*,$$

$$\text{Mh}(y) = \int_0^y \overline{q_y} dy^* / \int_0^1 \overline{q_y} dy^*,$$

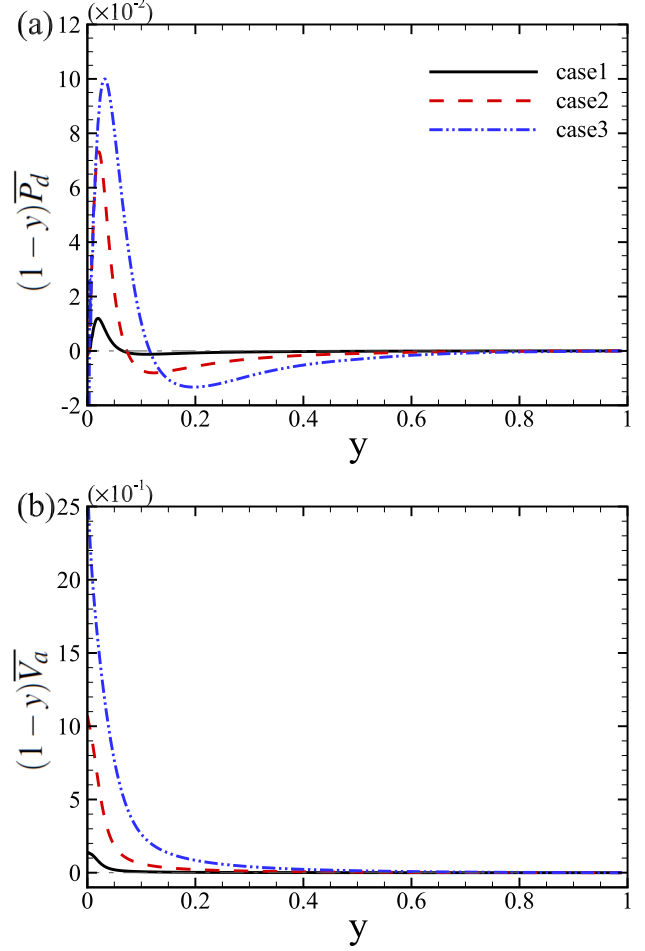


FIG. 5. The weighted distributions of (a) $(1-y)\overline{P_d}$ and (b) $(1-y)\overline{V_a}$ from the three cases. The quantities are normalized with $\rho_w C_p u_\tau T_w$.

$$\text{Pw}(y) = \int_0^y (1-y^*)\overline{P_d} dy^* / \int_0^1 (1-y^*)\overline{P_d} dy^*,$$

$$\text{Vw}(y) = \int_0^y (1-y^*)\overline{V_a} dy^* / \int_0^1 (1-y^*)\overline{V_a} dy^*.$$

For Th, as shown in Fig. 6(a), the cumulative contribution of the TH term increases as y increases, and it approaches to 90% of the total TH term when $y/h \gtrsim 0.6$ for all three cases. This means that the TH term is not restricted to the near-wall region but a whole field, and it is consistent with the normalized $C_v \overline{\rho T'' v''}$ distribution shown in Fig. 4(a).

Similarly, the cumulative contribution of the PW term, which is depicted in Fig. 7(a), also shows that the PW term is a global one. Due to the fact that $(1-y)\overline{P_d}$ has a positive peak in the near-wall region and a negative peak further away from the wall, Pw first increases with y and then decreases to 1 gradually. Differently from Th and Pw, Mh and Vw show a much better local behavior, as shown in Figs. 6(b) and 7(b), where more than 90% of the total MH and VW terms come from the near-wall region where $y/h \lesssim 0.2$ (inner region). In other words, most of the wall heat flux is generated in the inner region in the compressible turbulent channel flows with isothermal walls.

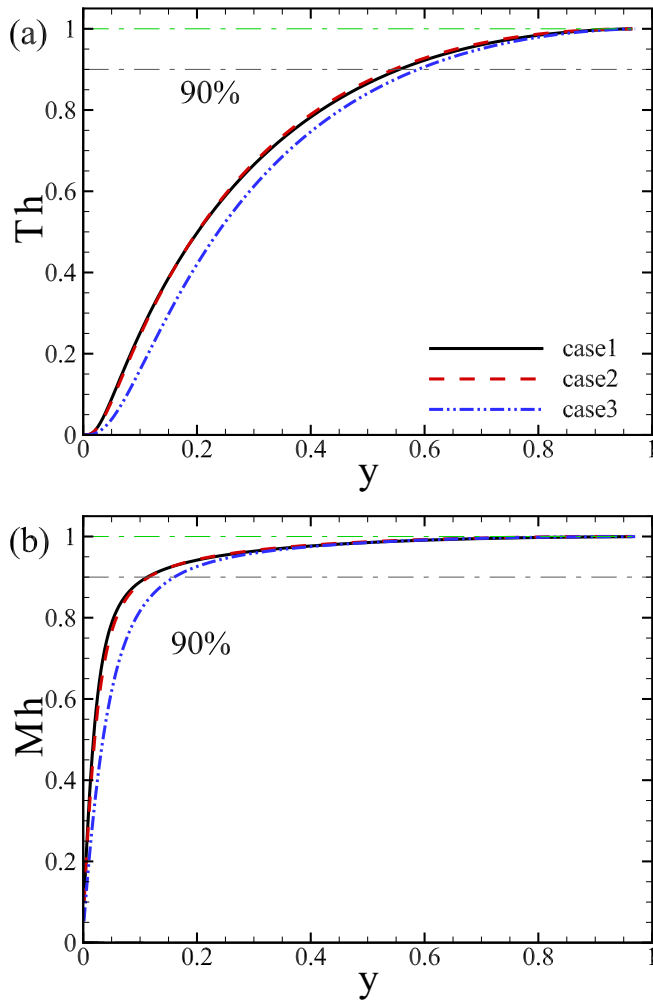


FIG. 6. Cumulative contributions of the integrands in the TH and MH terms from the three cases: (a) Th and (b) Mh.

V. CONCLUSIONS

To conclude, we have derived an exact relationship giving the contributions of different physical mechanisms to the wall heat flux, including the turbulent heat transfer (TH), the molecular heat transfer (MH), the pressure work (PW), and the viscous stress work (VW). Three DNSs with different Re and Ma are performed to validate the new decomposition, and very good agreement can be arrived between the decomposition formula and the direct estimation at the wall. The data also show that the VW term dominates the contribution (around 90%) in the total wall heat flux, and around 90%

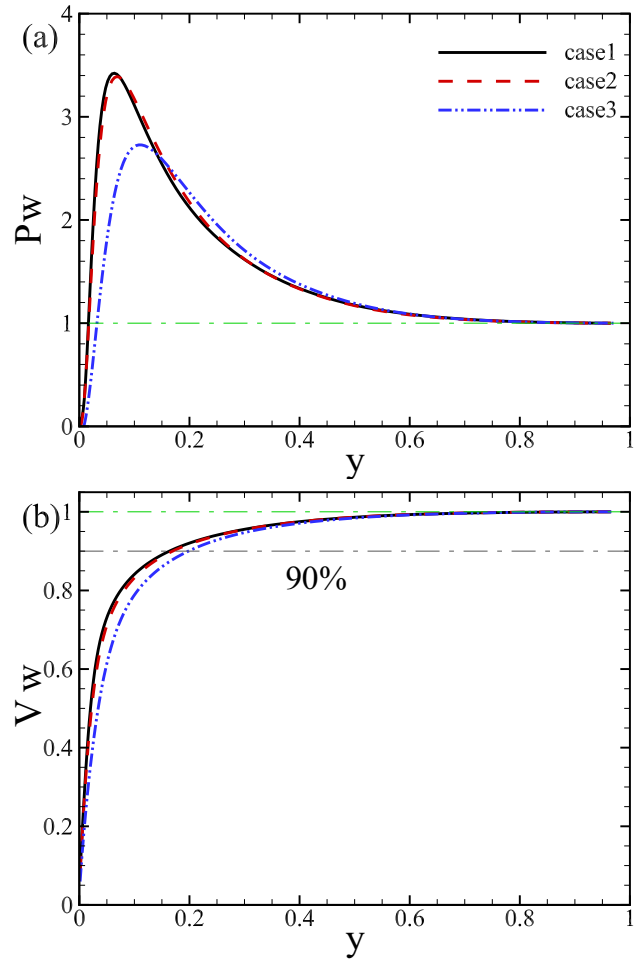


FIG. 7. Cumulative contributions of the integrands in the PW and VW terms from the three cases: (a) Pw and (b) Vw.

of the total VW term comes from the viscous stress work in the near-wall region ($y/h < 0.2$) in compressible turbulent channel flows with isothermal walls. In the future, the effect of Mach number and Reynolds number on different contribution terms will be analyzed with more DNS cases.

ACKNOWLEDGMENTS

We would like to thank Prof. Xinliang Li for the use of his OPENCFD code. We are also thankful for support from the National Natural Science Foundation of China (NSFC Grants No. 11822208, No. 11772297, and No. 91852205) and from the Fundamental Research Funds for the Central Universities of China.

- [1] Y. Liu, L. Zuo, and J. J. Wang, *Sci. China, Ser. G: Phys. Mech. Astron.* **53**, 915 (2010).
- [2] S. Chen, Y. C. Chen, Z. H. Xia, K. Qu, Y. Shi, Z. Xiao, Q. Liu, Q. Cai, F. Liu, C. Lee, R. Zhang, and J. Cai, *Sci. China, Ser. G: Phys. Mech. Astron.* **56**, 270 (2013).
- [3] P. Bradshaw, *Annu. Rev. Fluid Mech.* **9**, 33 (1977).
- [4] S. Lele, *Annu. Rev. Fluid Mech.* **26**, 211 (1994).

- [5] R. Friedrich, *Z. Angew. Math. Mech.* **87**, 189 (2007).
- [6] T. B. Gatski and J.-P. Bonnet, *Compressibility, Turbulence and High Speed Flow* (Academic Press, New York, 2013).
- [7] K. Fukagata, K. Iwamoto, and N. Kasagi, *Phys. Fluids* **14**, L73 (2002).
- [8] T. Gomez, V. Flutet, and P. Sagaut, *Phys. Rev. E* **79**, 035301(R) (2009).

- [9] N. Renard and S. Deck, *J. Fluid Mech.* **790**, 339 (2016).
- [10] M. Yoon, J. Ahn, J. Hwang, and H. Sung, *Phys. Fluids* **28**, 081702 (2016).
- [11] Y. Shi, Z. Xia, and S. Chen, *Phys. Fluids* **28**, 061702 (2016).
- [12] M. Yu, C. X. Xu, and S. Pirozzoli, *Phys. Rev. Fluids* **4**, 123402 (2019).
- [13] F. Laadhari, *Phys. Fluids* **19**, 038101 (2007).
- [14] H. Abe and R. Antonia, *J. Fluid Mech.* **798**, 140 (2016).
- [15] Z. Xia, Y. Shi, Q. Cai, and J. Gai, *J. Appl. Math. Mech. (Engl. Transl.)* **40**, 185 (2019).
- [16] W. Li, Y. Fan, D. Modesti, and C. Cheng, *J. Fluid Mech.* **875**, 101 (2019).
- [17] Y. Fan, W. Li, and S. Pirozzoli, *Phys. Fluids* **31**, 026103 (2019).
- [18] Y. Morinishi, S. Tamano, and K. Nakabayashi, *J. Fluid Mech.* **502**, 273 (2004).
- [19] M. Shadloo, A. Hadjadj, and F. Hussain, *Int. J. Heat Fluid Flow* **53**, 113 (2015).
- [20] X. Liang and X. Li, *Commun. Comput. Phys.* **17**, 189 (2015).
- [21] H. Kawamura, H. Abe, and Y. Matsuo, *Int. J. Heat Fluid Flow* **20**, 196 (1999).
- [22] L. Duan, I. Beekman, and M. Martin, *J. Fluid Mech.* **655**, 419 (2010).
- [23] Y. S. Zhang, W. T. Bi, F. Hussain, X. L. Li, and Z. S. She, *Phys. Rev. Lett.* **109**, 054502 (2012).
- [24] E. Hopkins and M. Inouye, *AIAA J.* **9**, 993 (1971).
- [25] P. G. Huang, G. N. Coleman, and P. Bradshaw, *J. Fluid Mech.* **305**, 185 (1995).
- [26] S. Ghosh, H. Foysi, and R. Friedrich, *J. Fluid Mech.* **648**, 155 (2010).
- [27] K. Fukagata, K. Iwamoto, and N. Kasagi, in *Proc. of the 4th Int. Symp. Turbulence and Shear Flow Phenomena* (Begell House Digital Library, Williamsburg, VA, June 27–29, 2005), pp. 307–312.
- [28] N. Kasagi, Y. Hasegawa, K. Fukagata, and K. Iwamoto, *J. Heat Transfer* **134**, 031009 (2012).
- [29] Y. Kametani, A. Kotake, K. Fukagata, and N. Tokugawa, *Phys. Rev. Fluids* **2**, 123904 (2017).
- [30] A. Mittal and S. S. Girimaji, *Phys. Rev. Fluids* **4**, 042601(R) (2019).
- [31] G. Gerolymos and I. Vallet, *J. Fluid Mech.* **757**, 701 (2014).
- [32] X. Liang and X. Li, *Sci. China, Ser. G: Phys. Mech. Astron.* **56**, 1408 (2013).
- [33] X. Chen, X. L. Li, and Z. Zhu, *Sci. China, Ser. G: Phys. Mech. Astron.* **62**, 064711 (2019).
- [34] G. Coleman, J. Kim, and R. Moser, *J. Fluid Mech.* **305**, 159 (1995).
- [35] D. Modesti and S. Pirozzoli, *Int. J. Heat Fluid Flow* **59**, 33 (2016).
- [36] A. Trettel and J. Larsson, *Phys. Fluids* **28**, 026102 (2016).
- [37] R. Moser, J. Kim, and N. Mansour, *Phys. Fluids* **11**, 943 (1999).